Supplementary Information for

Blocking the m^{6}Am methyltransferase PCIF1 releases STAT1-mediated Th1 immunity to potentiate cancer immunotherapy

Jiansong Huang[1,2#], Jing Zhou[1,2,3#*], Xiao Liu[4,5,6#], Xiaoxu Liu[7#], Ye Xiao[8#], Kai Li[8#], Chenbo Ding[9], Xuemin Cai[9], Wenli Mao[7], Changfen Xu[1,2], Yuxin Kong[10], Yu Deng[1,2], Xiaohan Song[1,2], Mei Yang[1,2], Daohai Du[4], Siqi Guo[4], Kaixian Chen[4,5], Cheng Luo[4,5,11], Chengqi Yi[8,12,13*], Shijie Chen[4,6*], Hua-Bing Li[1,7,9*]

[1] Center for Immune-Related Diseases at Shanghai Institute of Immunology, Ruijin Hospital, Shanghai Jiao Tong University School of Medicine, Shanghai, China.

[2] Shanghai Jiao Tong University School of Medicine-Yale Institute for Immune Metabolism, Shanghai Jiao Tong University School of Medicine, Shanghai, China.

[3] Key Laboratory of Cell Differentiation and Apoptosis of Chinese Ministry of Education, Shanghai Jiao Tong University School of Medicine, Shanghai, China

[4] State Key Laboratory of Drug Research, Shanghai Institute of Materia Medica, Chinese Academy of Sciences, Shanghai, China.

[5] University of Chinese Academy of Sciences, Beijing, China.

[6] Innovation Center for AI and Drug Discovery, School of Pharmacy. East China Normal University, Shanghai, China.

[7] Department of Geriatrics, Medical Center on Aging of Ruijin Hospital, Shanghai Jiao Tong University School of Medicine, Shanghai, China.

[8] Peking-Tsinghua Center for Life Sciences, Peking University, Beijing, China.

[9] Institute for Immunology and Pathogenesis, Chongqing Medical University, Chongqing, China.

[10] Department of Ophthalmology, Shanghai Key Laboratory of Orbital Diseases and Ocular Oncology, Ninth People's Hospital, Shanghai JiaoTong University School of Medicine, Shanghai, China.

[11] School of Pharmaceutical Sciences, State Key Laboratory of Functions and Applications of Medicinal Plants, Guizhou Medical University, Guiyang, China.

[12] State Key Laboratory of Protein and Plant Gene Research, School of Life Sciences, Peking

University, Beijing, China.

[13] Department of Chemical Biology and Synthetic and Functional Biomolecules Center, College of Chemistry and Molecular Engineering, Peking University, Beijing, China.

[#] These authors contributed equally to this work.

*Corresponding author: huabing.li@shsmu.edu.cn (H-B.L.), jingzhou@shsmu.edu.cn (J.Z.), sjchen@pharm.ecnu.edu.cn (S.C.), chengqi.yi@pku.edu.cn (C.Y.)

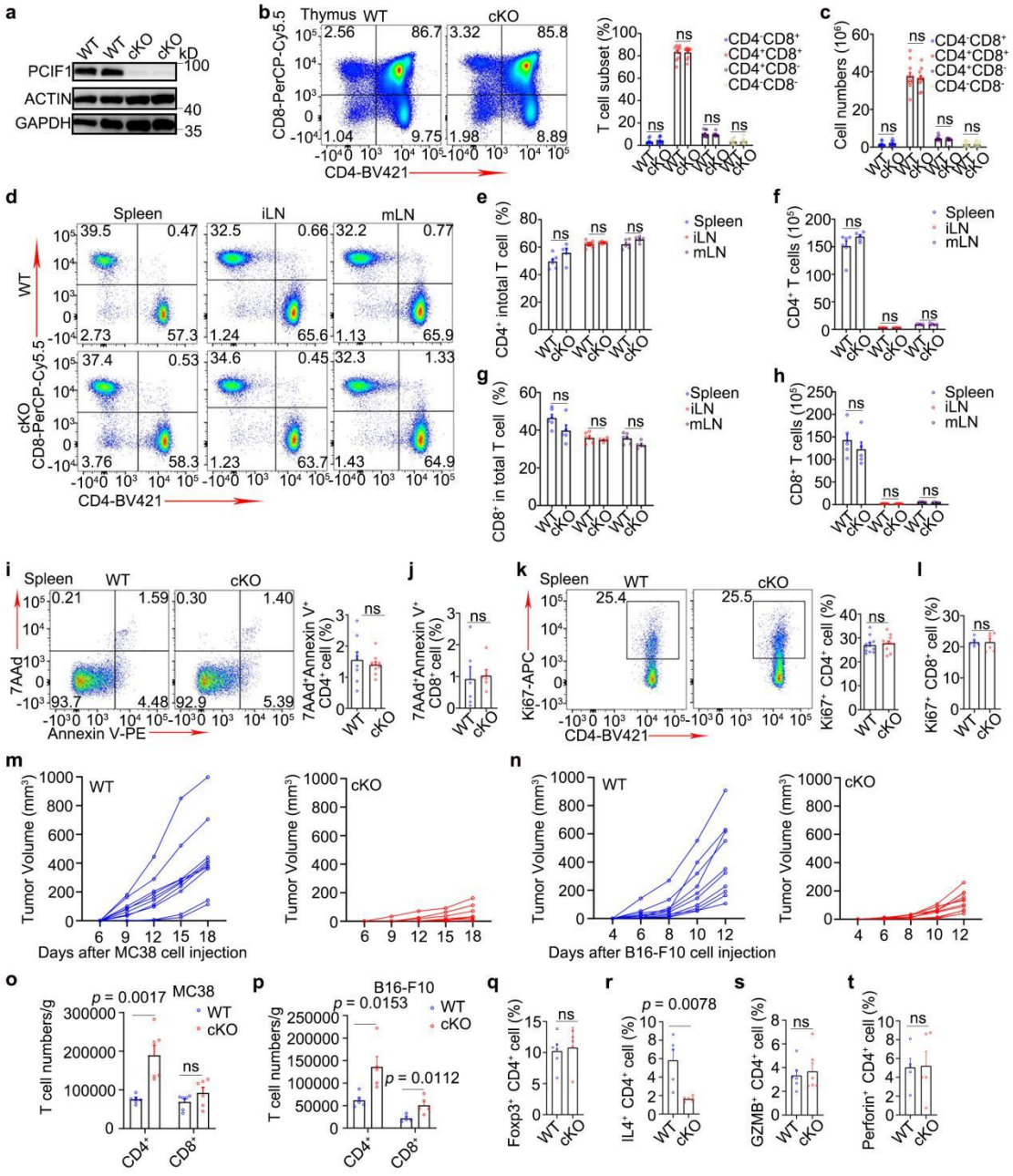

Supplementary Figure 1. PCIF1 deficiency in T cells does not alter steady-state immunity but enhances antitumor responses.

a, Immunoblots of PCIF1 protein levels in naïve $CD4^+$ T cells from wild-type and PCIF1 conditional knockout mice (n=3). **b**, Representative dot plots (left) and quantification (right) of T cell subset composition in the thymus of WT and cKO mice (n=11). **c**, Quantification of T cell subset numbers in the thymus (n=11). **d**, Representative dot plots of T cell subsets from the spleen, inguinal lymph nodes (iLN), and mesenteric lymph nodes (mLN) of WT and cKO mice.

e-h, Quantification of the frequency and absolute numbers of $CD4^+$ (**e**, **f**) and $CD8^+$ T cells (**g**, **h**) in spleen, iLN, and mLN from WT and cKO mice (WT Group n=6, cKO Group n=5). **i**, Representative dot plots (left) and quantification (right) of Annexin V/7-AAD staining on splenic $CD4^+$ T cells from WT and cKO mice at steady-state (WT Group n=8, cKO Group n=10). **j**, Quantification of Annexin V/7-AAD staining on splenic $CD8^+$ T cells from WT and cKO mice at steady-state (n=6). **k**, Representative dot plots (left) and quantification (right) of Ki67 staining on splenic $CD4^+$ T cells from WT and cKO mice at steady-state (n=12). **l**, Quantification of Ki67 staining on splenic $CD8^+$ T cells from WT and cKO mice at steady-state (n=6). **m**, **n**, Tumor growth curves of MC38 (**m**) and B16-F10 (**n**) in WT or cKO mice (WT Group n=10, cKO Group n=11). **o**, Quantification of tumor-infiltrating T cell numbers in the MC38 model (n=6). **p**, Quantification of tumor-infiltrating T cell numbers in the B16-F10 model (n=5). **q**, **r**, Quantification of Treg (**q**) and Th2 (**r**) frequencies among tumor-infiltrating $CD4^+$ T cells at day 18 in the B16-F10 model (WT Group n=6, cKO Group n=5). **s**, **t**, Quantification of granzyme B (**s**) and perforin (**t**) expression in tumor-infiltrating $CD4^+$ T cells isolated from WT and cKO mice at day 18 from the B16-F10 model (**s** Group n=6, **t** Group n=5). Each n represents an individual mouse(**a-t**). Error bars represent mean ± SEM; two-tailed, unpaired t-test (**b**, **c**, **e-l**, **o-t**); two-way ANOVA (**m**, **n**). ns (no significance); *p*-values are shown on the graphs, and *p*-values < 0.0001 are reported as such.

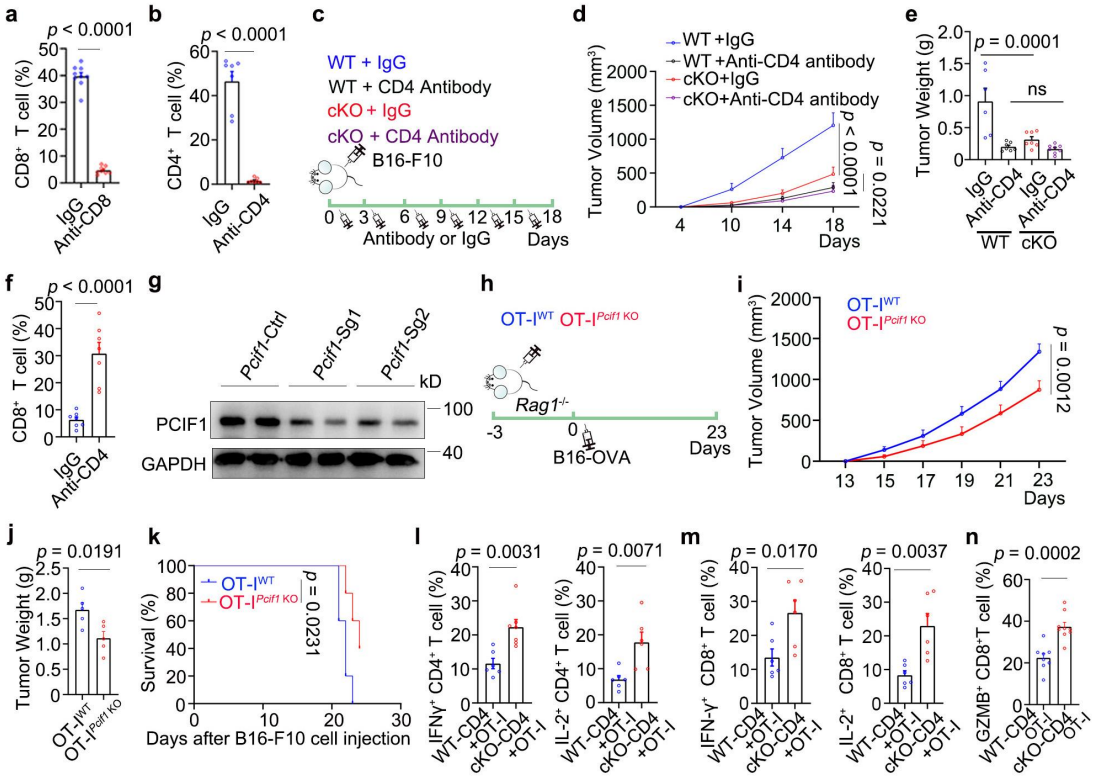

Supplementary Figure 2. PCIF1 deficiency in CD4⁺ T cells enhances CD8⁺ T cell-mediated antitumor immunity.

a, Proportion of $CD8^+$ T cells among $CD3^+$ T cell populations in draining lymph nodes at 3 days after injection of anti-CD8 or control IgG (WT Group n=9, cKO Group n=8). **b**, Proportion of $CD4^+$ T cells among $CD3^+$ T cells in draining lymph nodes 3 days after injection of anti-CD4 or control IgG (n=7). **c-e**, WT or cKO mice were intraperitoneally injected with anti-CD4 antibody following B16-F10 inoculation (**c**). Tumor growth curves (**d**) and tumor weights on day 18 (**e**) are shown (WT Group n=6, cKO+CD4 depletion Group n=8,other Group n=7). **f**, Proportion of $CD8^+$ T cells among tumor-infiltrating $CD3^+$ T cells after anti-CD4 or control IgG treatment (n=7). **g**, Immunoblots of PCIF1 protein levels in Contol (Ctrl) or *Pcif1*-sgRNA OT-II $CD4^+$ T cells (n=2). **h-k**, WT or $PCIF1^{-/-}$ $CD8^+$ OT-I cells were adoptively transferred into *Rag1*$^{-/-}$ mice, followed by B16-OVA inoculation (**h**). Tumor growth curves (**i**), tumor weights (**j**) and survival curves (**k**) are shown (n=5). **l**, **m**, WT or $PCIF1^{-/-}$ $CD4^+$ T cells, along with OT-I cells, were adoptively transferred into *Rag1*$^{-/-}$ mice. The mice were subcutaneously inoculated with B16-OVA cells to initiate tumor growth. Quantification of IFN-γ-positive (left) and IL-2-positive (right) $CD4^+$ T cells (**l**) and $CD8^+$ T cells (**m**) within the tumor is shown (WT n=6, cKO n=7). **n**,

Quantification of granzyme B^+ tumor-infiltrating $CD8^+$ T cells (WT n=8, cKO n=9). Each n represents an individual mouse (**a-n**). Error bars represent mean ± SEM; two-tailed, unpaired *t*-test(**a**, **b** , **f**, **j**, **l**-**n**); one-way ANOVA (**e**); two-way ANOVA (**d, i**); log-rank test (**k**). ns (no significance); *p*-values are shown on the graphs, and *p*-values < 0.0001 are reported as such.

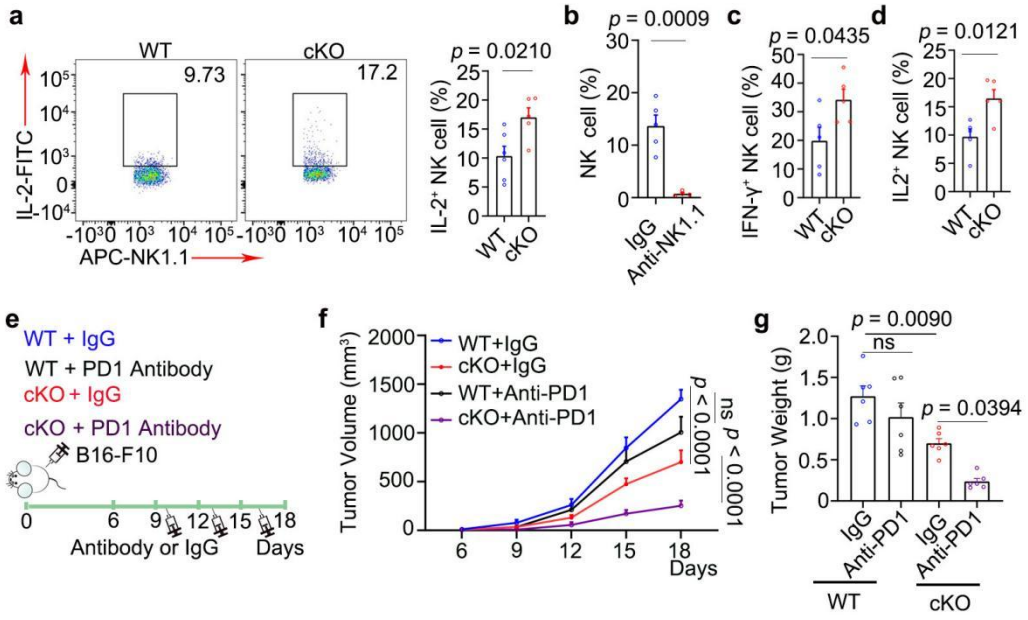

Supplementary Figure 3. PCIF1 deletion potentiates PD-1 blockade therapy.

a, Representative dot plots (left) and quantification (right) of IL-2$^+$ NK cells within the tumor (WT n=6, cKO n=5). **b**, Ratios of tumor-infiltrating NK cells among CD3$^-$ populations 3 days after injection of anti-NK1.1 or control IgG (WT n=5, cKO n=4). **c**,**d**, WT or PCIF1$^{-/-}$ CD4$^+$ T cells were adoptively transferred into *Rag1*$^{-/-}$ mice. The mice were subcutaneously inoculated with B16-F10 cells to initiate tumor growth. Quantification of IFN-γ$^+$ (**c**) and IL-2$^+$ (**d**) tumor-infiltrating CD4$^+$ T cells 16 days after adoptive transfer and B16-F10 inoculation (n=5). **e-g**, WT and cKO mice bearing established B16-F10 tumors were treated with anti-PD-1 antibody. Tumor growth curves (**f**) and final weights (**g**) are shown (n=6). Each n represents an individual mouse (**a-g**). Error bars represent mean ± SEM; two-tailed, unpaired *t*-test(**a-d**); one-way ANOVA (**g**); two-way ANOVA (**f**); ns (no significance); *p*-values are shown on the graphs, and *p*-values < 0.0001 are reported as such.

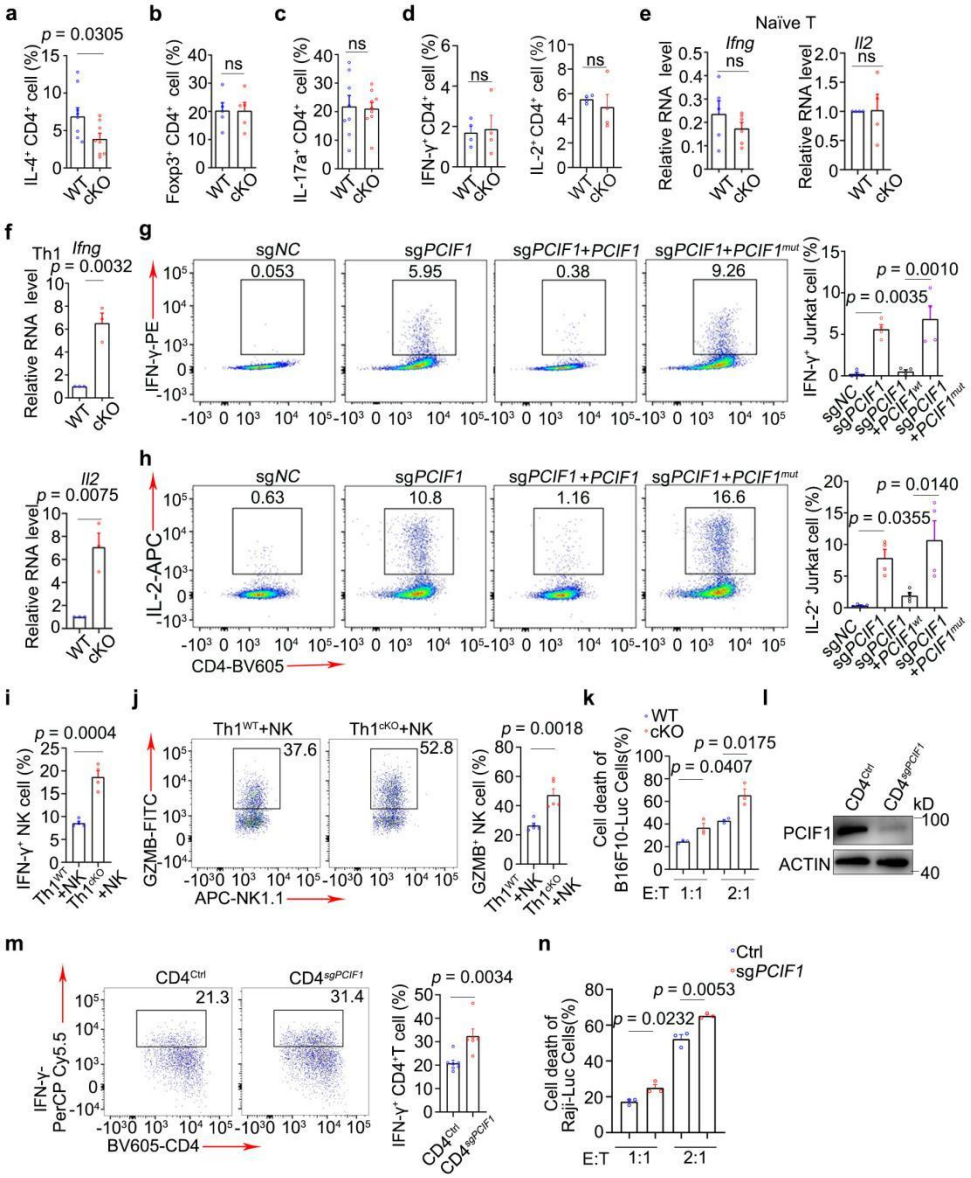

Supplementary Figure 4. PCIF1 regulates Th1 function in a catalytic activity-dependent manner.

a, Quantification of IL-4 expression in CD4$^+$ T cells after Th2 differentiation (n=8). **b**, Quantification of Foxp3 expression in CD4$^+$ T cells after Treg differentiation (n=5). **c**, Quantification of IL-17a expression in CD4$^+$ T cells after Th17 differentiation (WT n=8, cKO n=9). **d**, Quantification of IFN-γ (left) and IL-2 (right) expression in naïve CD4$^+$ T cells (n=4). **e**, **f**, qPCR analysis of *Ifng* (left) and *Il2* (right) expression in naïve (**e**) and Th1-differentiated (**f**) CD4$^+$ cells from WT and cKO mice (**e**: WT Group n=5, cKO Group n= 6; **f**: n=4). **g**, **h**, Representative dot plots (left) and quantification (right) of IFN-γ (**g**) and IL-2 (**h**) expression in *PCIF1*-KO Jurkat

cells rescued with WT (NPPF) or catalytic mutant PCIF1 (APPA) (n=4). **i**, Quantification of IFN-γ^+ NK cells after co-culture with *in vitro*-polarized Th1 cells (n=4). Naïve $CD4^+$ T cells isolated from the spleen of cKO mice and differentiated into a Th1 phenotype under *in vitro* conditions for three days, and Th1 and NK cells were co-cultured for 24 hours. **j**, Representative dot plots (left) and quantification (right) of granzyme B^+ NK cells after co-culture (n=5). **k**, *In vitro* cytotoxic activity of WT/cKO $CD4^+$ T cells and NK cells co-culture system against B16-luciferase cells at various effector-to-target ratios after 48 hours co-culture (n=3). **l**, Immunoblots of PCIF1 in control or *PCIF1*-sgRNA human $CD4^+$ T cells (n=2). **m**, Representative flow cytometry plots (left) and quantification (right) of IFN-γ^+ human $CD4^+$ T cells from control and *PCIF1*-sgRNA treatment after Th1 polarization (WT Group n=7, cKO Group n=6). **n**, *In vitro* cytotoxicity of co-cultured human control or *PCIF1*-deficient Th1 cells and NK cells against Raji-luciferase cells at the indicated effector-to-target (E:T) ratios after 24 hours co-culture (n=3). Each n represents biologically independent cell samples (**g-i**, **l-n**) or an individual mouse (**a-f**, **j-k**). Error bars represent mean ± SEM; two-tailed, unpaired *t*-test(**a-f**, **i-k**, **m**, **n**); one-way ANOVA (**g**, **h**); ns (no significance); *p*-values are shown on the graphs, and *p*-values < 0.0001 are reported as such.

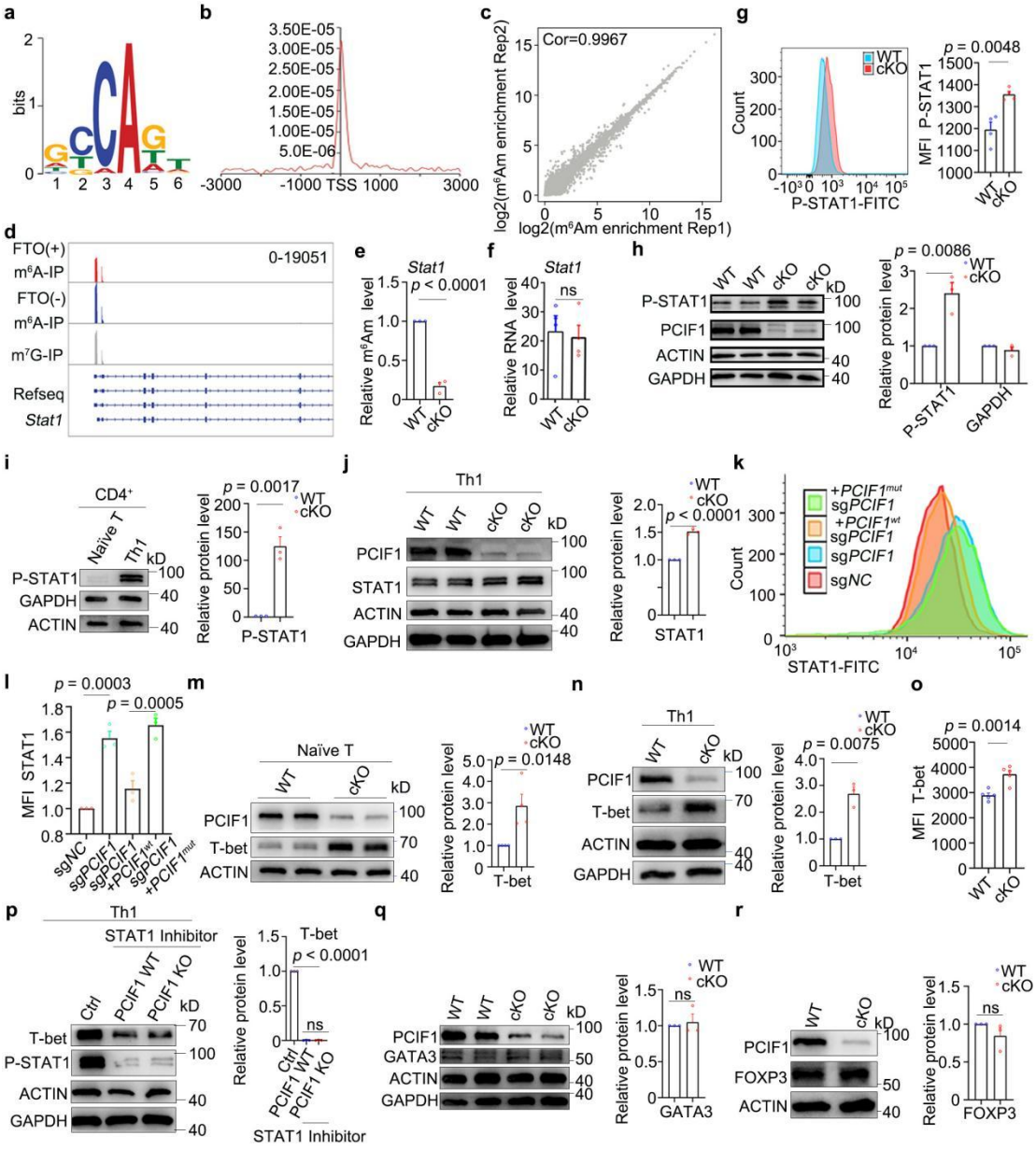

Supplementary Figure 5. PCIF1 regulates *Stat1* translation.

a, Motif analysis of m^{6}Am peaks in naïve CD4$^+$ T cells. **b**, Metaplot showing overlap of m^{6}Am sites with cap-analysis of gene expression (CAGE)-defined transcription start sites (TSSs). **c**, Correlation plot between two biological replicates (R=0.9967). **d**, Genome browser view of an m^{6}Am peak on *Stat1* mRNA from naïve CD4$^+$ T cells. **e**, m^{6}Am-seq analysis of m^{6}Am levels on *Stat1* mRNA in naïve CD4$^+$ T cells from WT and PCIF1 cKO mice (n=3). **f**, qPCR analysis of *Stat1* mRNA levels in naïve CD4$^+$ T cells from WT and cKO mice (n=4). **g**, Representative histograms (left) and quantification (right) of P-STAT1 levels in naïve CD4$^+$ T cells by flow

cytometry from WT or cKO mice (n=4). **h**, Immunoblots (left) and quantification (right) of P-STAT1 protein in naïve $CD4^+$ T cells from WT or cKO mice (n=3). **i**, Immunoblots (left) and quantification (right) of P-STAT1 protein in naïve $CD4^+$ T and Th1 cells (n=3). **j**, Immunoblots (left) and quantification (right) of STAT1 protein in Th1 cells (n=3). **k**, **l**, Representative histograms (**k**) and quantification (**l**) of STAT1 protein levels in *PCIF1*-KO Jurkat cells and those rescued with WT (NPPF) or catalytic mutant PCIF1 (APPA) (n=3). **m**, Immunoblots (left) and quantification (right) of T-bet protein in naïve $CD4^+$ T cells (n=4). **n**, Immunoblots (left) and quantification (right) of T-bet protein in Th1 cells (n=3). **o**, Quantification of T-bet levels in tumor-infiltrating $CD4^+$ T cells (n=5). **p**, Immunoblots (left) and quantification (right) of T-bet protein in Th1 cells treated with a STAT1 inhibitor (n=3). **q**, Immunoblots (left) and quantification (right) of GATA3 protein in naïve $CD4^+$ T cells (n=3). **r**, Immunoblots (left) and quantification (right) of FOXP3 protein in naïve $CD4^+$ T cells (n=3). Each n represents biologically independent cell samples (**k**, **l**) or an individual mouse (**e-j**, **m-r**). Error bars represent mean ± SEM; two-tailed, unpaired *t*-test (**e-j**, **m-r**); one-way ANOVA (**l**, **p**); ns (no significance); *p*-values are shown on the graphs, and *p*-values < 0.0001 are reported as such.

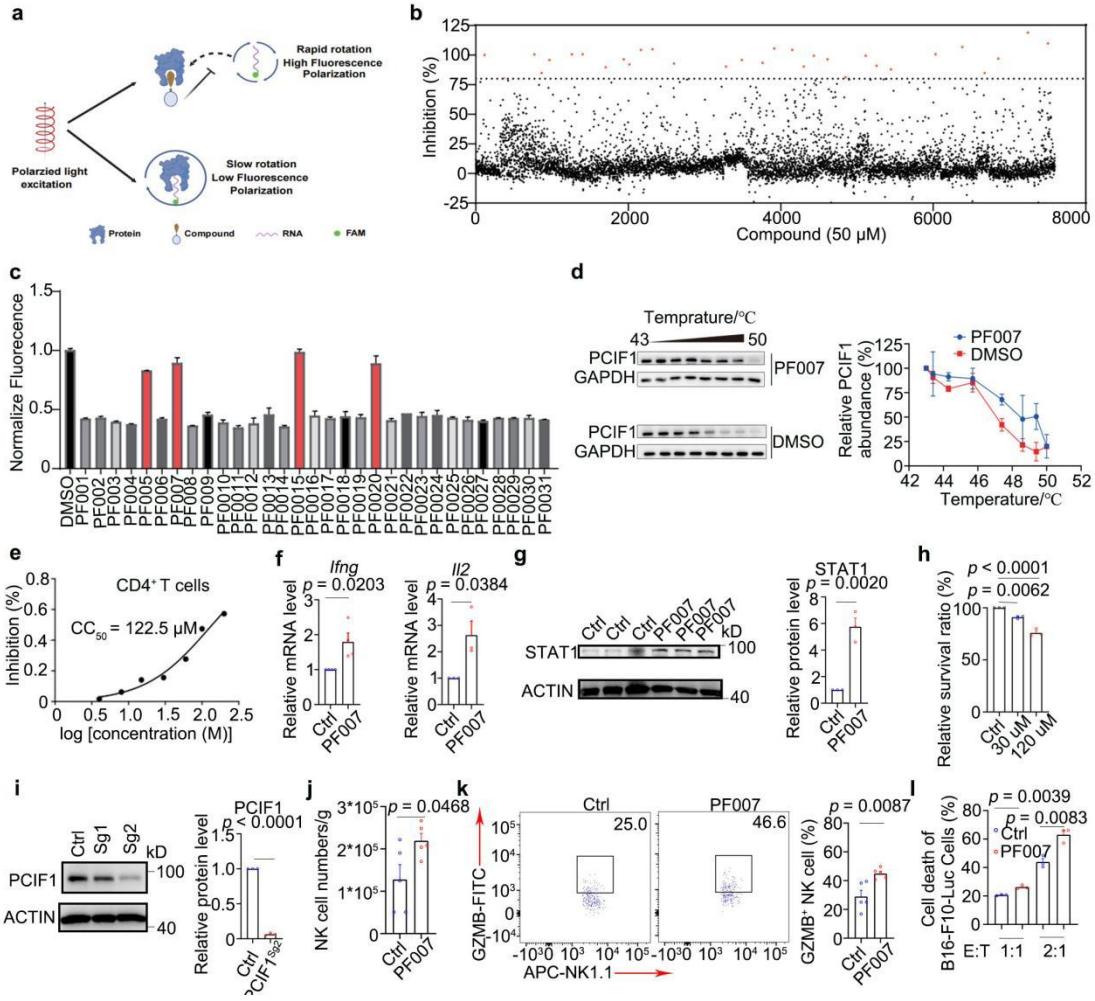

Supplementary Figure 6. Screening of small molecule inhibitors targeting PCIF1.

a, Schematic of the screening process for PCIF1 inhibitors,created in BioRender. Xiao, L. (2026) https://BioRender.com/u85x792. **b**, Results of high-throughput screening. Primary 'hit' compounds are in red. **c**, Fluorescence intensity of Fam-labeled RNA incubated with 31 'hit' compounds (n=2). Secondary 'hit' compounds are highlighted in red. Error bars represent mean ± SEM. **d**, Cellular thermal shift assay (CETSA) of Jurkat cells treated with PF007 (60 μM) or DMSO. Immunoblots (left) and quantification (right) of endogenous PCIF1 (n=3). **e**, Cytotoxicity (CC_{50}) of PF007 in mouse $CD4^+$ T cells (n=3). **f**, qPCR analysis of *Ifng* (n=4) and *Il2* (n=3) expression in PF007-treated (30 μM) Th1 cells. **g**, Immunoblots (left) and quantification (right) of STAT1 protein in Jurkat cells treated with PF007 (60 μM, 72 hours) (n=3). **h**, *In vitro* cytotoxic activity of PF007 against B16-luciferase cells at 120 μM and 30 μM after 48 hours

treatment(n=3). **i**, Knockout of PCIF1 in B16-F10 cells using sgRNA, with knock-out efficiency confirmed by immunoblotting (n=3). **j**, B16-F10 cells were injected subcutaneously into WT and cKO mice, and PF007 was administered intraperitoneally every two days after B16-F10 subcutaneous injection. The numbers of NK cells within the tumors are shown (n=5). **k**, Representative dot plots (left) and quantification (right) of granzyme B^+ NK cells within the tumors (n=5). **l**, *In vitro* cytotoxicity of co-cultured WT/cKO Th1 cells and splenic NK cells against B16-luciferase tumor cells at indicated effector-to-target (E:T) ratios after 48 hours (n=3). Each n represents biologically independent RNA oligos samples (**c**), cell samples (**d**, **e**, **g**, **h**, **i**), or an individual mouse (**f**, **j**-**l**). Data in **c** represent the aggregated results of two independent experiments**, d** (right) represent the aggregated results of three independent experiments, **d** (left) and **e**-**l** represent one of three independent experiments and are shown as the means ± SEM; Error bars represent mean ± SEM; two-tailed, unpaired *t*-test (**f**, **g**, **i-l**); one-way ANOVA (**h**) *p*-values are shown on the graphs, and *p*-values < 0.0001 are reported as such.

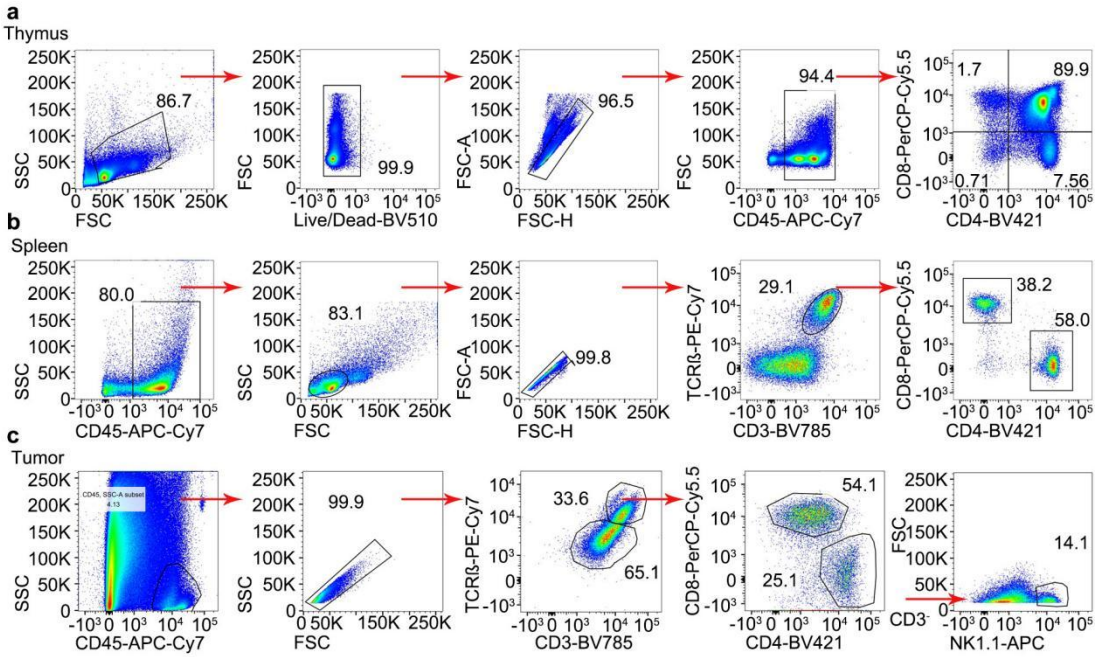

Supplementary Figure 7. Representative flow cytometry gating strategy.

a-c, Flow cytometry gating strategy for immune cell subsets in (**a**) thymus, (**b**) spleen, and (**c**) tumor.

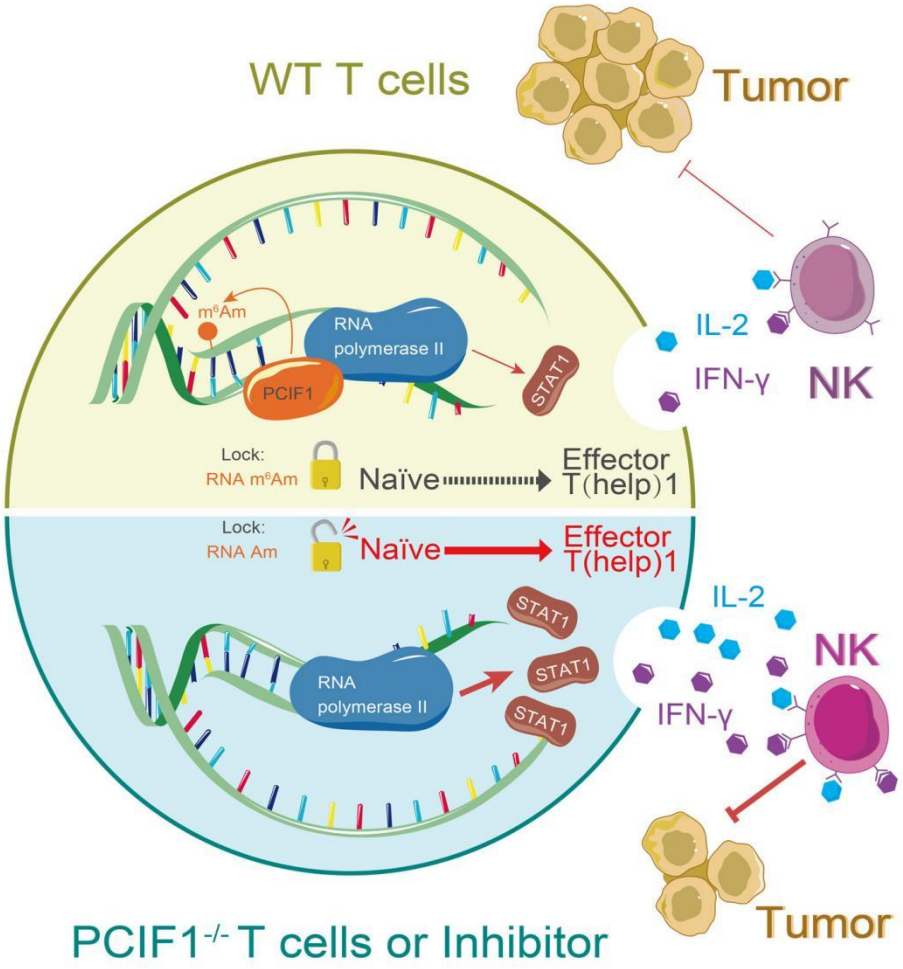

Supplementary Figure 8. Schematic model: mRNA m^{6}Am methylation maintains T cell quiescence

In naïve CD4$^+$ T cells, the m^{6}Am methyltransferase PCIF1 catalyzes m^{6}Am modification on nascent transcripts, establishing a post-transcriptional checkpoint that reinforces translational repression and safeguards T cell quiescence. Upon stimulation, rapid loss of m^{6}Am on *Stat1* mRNA alleviates this repression, enabling rapid Th1 differentiation and enhancing NK cell-mediated antitumor immunity. Our findings identify PCIF1 inhibition as a potential strategy for cancer immunotherapy. Supplementary Figure 8 includes elements adapted from Servier Medical Art (https://smart.servier.com), which is licensed under CC BY 3.0 (https://creativecommons.org/licenses/by/3.0/).

Supplementary Table 1. Small molecule screening data

Category	Parameter	Description
Assay	Type of assay	In vitro
	Target	PCIF1
	Primary measurement	The polarization of emitted light in FP
	Key reagents	PCIF1; FAM-RNA oligo
	Assay protocol	FP assay was performed at 25 °C in 384-well plates and the reaction volume was 40 μL. 150 nM PCIF1 was pre-incubated with 50 μM compounds for 30 minutes, and then FP-signals were detected immediately by Envision Readers (PerkinElmer) after adding 50 nM FAM-labeled. The results were analyzed in GraphPad Prism 8.0.
	Additional comments	
Library	Library size	7,595 compounds
	Library composition	Known bioactives and drug-like molecules
	Source	Compounds obtained from commercial sources
	Additional comments	
Screen	Format	384-well plates
	Concentration(s) tested	50 μM
	Plate controls	
	Reagent/ compound dispensing system	
	Detection instrument and software	EnVision multilabel reader （PerkinElmer）, EnVision Manager(Version 1.13.3009.1401)
	Assay validation/QC	Z' score: 0.73
	Correction factors	
	Normalization	
	Additional comments	
Post-HTS analysis	Hit criteria	The compounds that caused a decrease in fluorescence polarization by more than 80%.were selected
	Hit rate	0.4%
	Additional assay(s)	PTS; SPR; ITC
	Confirmation of hit purity and structure	
	Additional comments	

Supplementary Figure 1 a

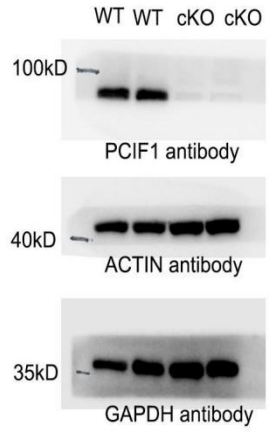

Supplementary Figure 2 g

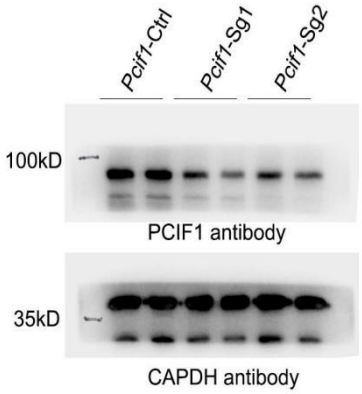

Supplementary Figure 4 l

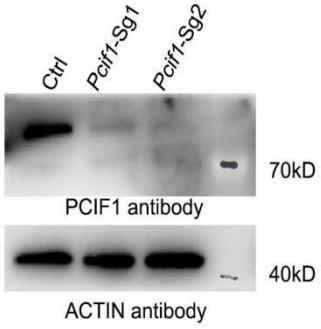

Supplementary Figure 5 h

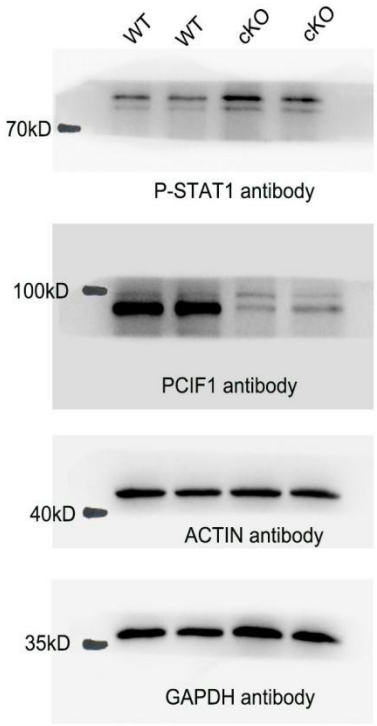

Supplementary Figure 5 i

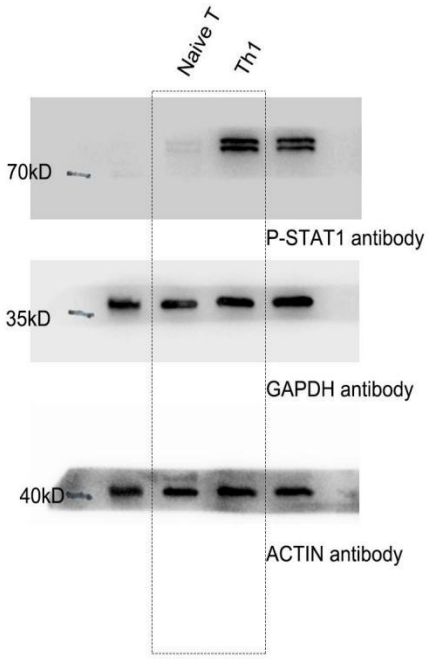

Supplementary Figure 5 j

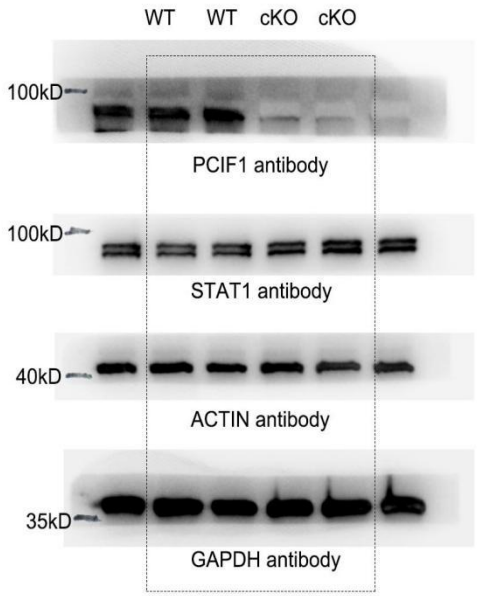

Supplementary Figure 5 m

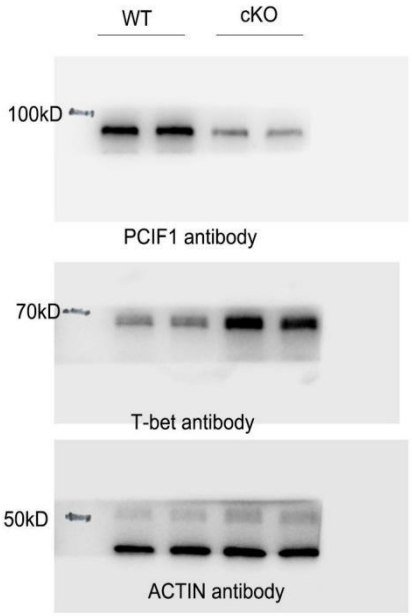

Supplementary Figure 5 n

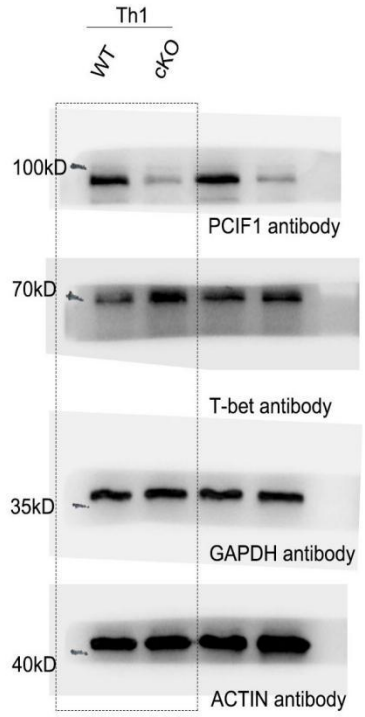

Supplementary Figure 5 p

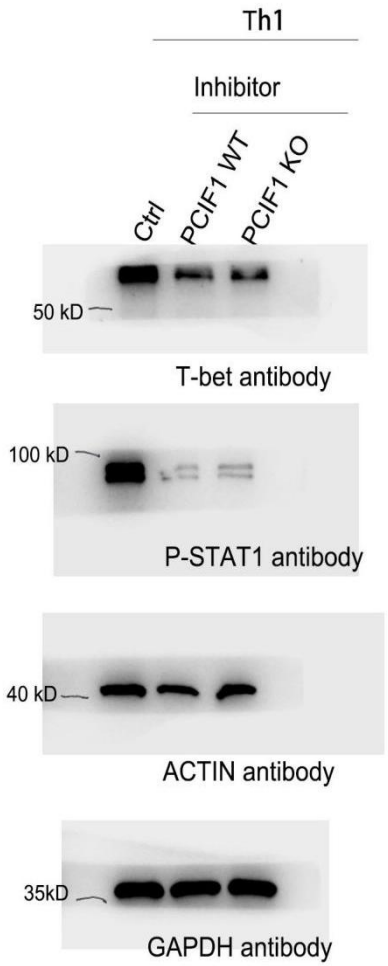

Supplementary Figure 5 q

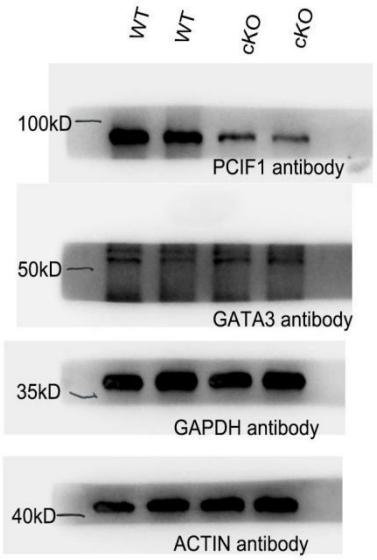

Supplementary Figure 5 r

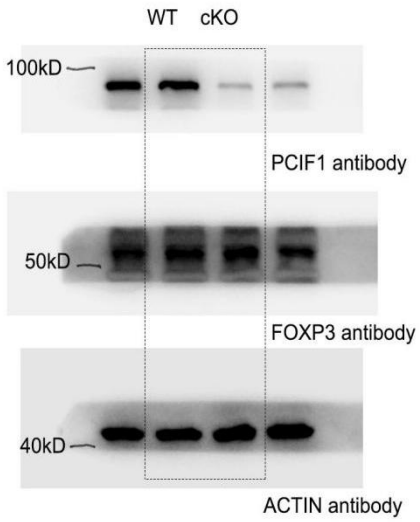

Supplementary Figure 6 g

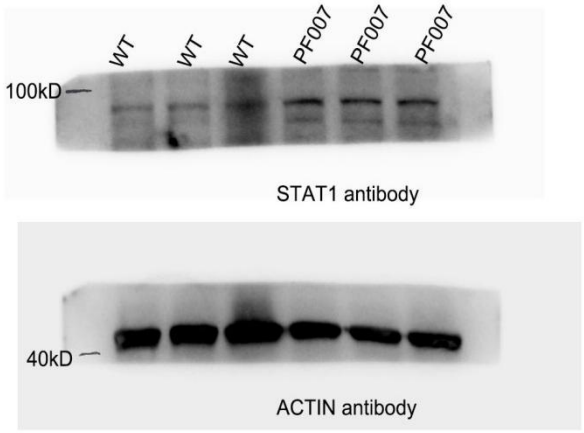

Supplementary Figure 6 i